

Gust Response of Free-Falling Permeable Plates

Bose, Chandan; Viola, Ignazio Maria

DOI:

[10.48550/arXiv.2304.04317](https://doi.org/10.48550/arXiv.2304.04317)

License:

Creative Commons: Attribution (CC BY)

Document Version

Other version

Citation for published version (Harvard):

Bose, C & Viola, IM 2023 'Gust Response of Free-Falling Permeable Plates' arXiv.
<https://doi.org/10.48550/arXiv.2304.04317>

[Link to publication on Research at Birmingham portal](#)

General rights

Unless a licence is specified above, all rights (including copyright and moral rights) in this document are retained by the authors and/or the copyright holders. The express permission of the copyright holder must be obtained for any use of this material other than for purposes permitted by law.

- Users may freely distribute the URL that is used to identify this publication.
- Users may download and/or print one copy of the publication from the University of Birmingham research portal for the purpose of private study or non-commercial research.
- User may use extracts from the document in line with the concept of 'fair dealing' under the Copyright, Designs and Patents Act 1988 (?)
- Users may not further distribute the material nor use it for the purposes of commercial gain.

Where a licence is displayed above, please note the terms and conditions of the licence govern your use of this document.

When citing, please reference the published version.

Take down policy

While the University of Birmingham exercises care and attention in making items available there are rare occasions when an item has been uploaded in error or has been deemed to be commercially or otherwise sensitive.

If you believe that this is the case for this document, please contact UBIRA@lists.bham.ac.uk providing details and we will remove access to the work immediately and investigate.

Gust Response of Free-Falling Permeable Plates

Chandan Bose, Ignazio Maria Viola*
School of Engineering, Institute for Energy Systems
University of Edinburgh, Edinburgh, EH9 3FB, UK
* i.m.viola@ed.ac.uk

April 18, 2023

Abstract

This paper investigates the effect of transverse gusts on the flight dynamics and descent velocity of two-dimensional free-falling permeable plates. Two-way coupled fluid-structure interaction simulations are carried out for a range of Galilei number (Ga) from 10 and 50, nondimensional mass (m) from 0.5 to 2, and a fixed Darcy number of 10^{-4} . The present results show that the plate falls steadily in quiescent flow at the lowest Ga and m values, whereas fluttering and tumbling are observed for increased Ga and/or m . A transverse (horizontal) gust temporarily decreases the descent velocity of the plate in the transient regime and can also uplift the plate. The gust effect increases with the gust ratio, Ga and m . The underlying uplifting mechanism is not directly related to the permeability, and it is thus likely to occur also for impermeable bodies. The present findings might provide insights to interpret the effect of turbulence on the terminal velocity of free-falling bodies and inform the design of insect-scale flyers passively transported by the wind.

1 Introduction

The dynamics of the unconstrained flight of falling objects under gravitational acceleration has garnered a long-standing research interest (Ern *et al.*, 2012) due to their multi-fold applications in plant biology (Cummins *et al.*, 2018), meteorology (Kajikawa, 1982), and engineering (Marchildon *et al.*, 1964; Viets & Lee, 1971). The recent developments of distributed sensor network systems made of bio-inspired insect-scale flying sensors for environment monitoring have further increased the interest on the aerodynamics of free-falling bodies (Cummins *et al.*, 2018; Kim *et al.*, 2021; Yoon *et al.*, 2022; Iyer *et al.*, 2022; Wiesemüller *et al.*, 2022).

The nondimensional groups that govern the physics of free-falling bodies are the dimensionless moment of inertia I^* , the Reynolds number Re , and the body's geometry, e.g. the aspect ratio (Willmarth *et al.*, 1964; Field *et al.*, 1997). Willmarth *et al.* (1964) and Smith (1971) were among the first studies to experimentally identify the range of Re and I^* for which discs and plates, respectively, fall steadily, flutter, or tumble. Later, Field *et al.* (1997) experimentally identified a chaotic regime for high Re and I^* .

The effect of the porosity, which is the void fraction of the circumscribed projected area of the body, and of the nondimensional permeability, or Darcy number Da , which is a measure of the ease of passage of fluid through the surface circumscribing the body, is to stabilise the wake. Castro (1971) was the first to show that at high Re ($Re > 2.5 \times 10^4$), the unstable wake of porous plates forms a separated vortex dipole in the time average sense. For sufficiently low Re and Da , the wake is stable and a steady vortex dipole is observed (Ledda *et al.*, 2018; Bose & Viola, 2023). The dipole also exists for lower incidences than $\pi/2$, and nodes and saddles merge, annihilating the vortex dipole at a critical incidence that depends on Da (Bose & Viola, 2023).

The three-dimensional equivalent of the vortex dipole is a Separated Vortex Ring (SVR), which was first observed numerically by Cummins *et al.* (2017) in the wake of permeable disks, and then experimentally in the wake of the filamentous pappus of the dandelion diaspore (Cummins *et al.*, 2018). Ledda *et al.* (2019) showed that there is a limiting porosity, above which the wake of bristled disks is unconditionally stable.

The flight dynamics of free-falling porous and permeable objects is yet to be fully understood, but recent works suggest that porosity and permeability stabilise the kinematics of the free-falling body. Vincent *et al.* (2016) demonstrated that a central hole stabilises the free-fall of disc-shaped impervious bodies by forming a secondary vortex ring inside of that formed by the external edge of the body. The inner and outer diameter ratio has a significant impact on the falling trajectory as well as the flow structures in the wake (Bi *et al.*, 2022).

Disks with multiple holes were tested by Zhang *et al.* (2023), who found that the amplitude of the horizontal displacement of the free-falling kinematics is lower than those of impervious disks with the same Re and I^* . Lee *et al.* (2020) experimentally showed that bristled disks tend to reach a steady fall faster than impervious disks after they are released. Stability analysis reveals that permeability stabilises the modes dominated by wake oscillations (Vagnoli *et al.*, 2023).

The effect of permeability on the terminal velocity was investigated by Rezaee & Sadeghy (2019). The study shows that the terminal velocity of elliptic bodies increases substantially as the permeability is higher than a given threshold. This is consistent with the study of Cummins *et al.* (2017), which shows that the drag of a permeable disk is about constant for low Da , while it decreases asymptotically above a given threshold. However, permeability is exploited in nature by bristled diaspores such as that of the dandelion to decrease the mass and the wing loading and, in turn, the terminal velocity (Viola & Nakayama, 2022). Therefore, from an engineering perspective, minimum terminal velocity is achieved by increasing the permeability up to or just past the threshold, where the drag decreases asymptotically. Bose & Viola (2023) and Cummins *et al.* (2017) found that such threshold is approximately $Da = 10^{-4}$ on plates at $Re = 30$ and disks at $10 \leq Re \leq 130$, respectively. For this reason, we consider a constant permeability of $Da = 10^{-4}$ throughout this study.

Recent studies on bristled wings show that porosity mitigates but does not suppress the gust response. For example, Lee & Kim (2021) showed that, when subjected to a single intermittent gust with a sinusoidal velocity profile, the flow leakage through the gaps of two-dimensional (2D) bristled plates alleviates the unsteadiness of the aerodynamic loading. Galler & Rival (2021) experimentally investigated near-spherical bristled milkweed seeds and reported a transient peak drag force in response to a streamwise gust.

To the best of the authors' knowledge, the effect of transverse gusts on free-falling plates, either permeable or impermeable, has never been investigated. To that end, we first investigate the kinematics of free-falling plates after imposing an initial horizontal perturbation. Thereafter, we study the effect of a transverse velocity increase on the terminal velocity. We consider only conditions where the plate falls steadily in quiescent flow, such that the plate has no linear nor angular acceleration when the gust begins. For an impervious plate, this would require $O(1) < Re < O(10)$ (Saha, 2007; Ledda *et al.*, 2018; Bose & Viola, 2023), where the viscous effects are likely to mitigate some of the inertial effects that we aim to explore. Therefore, to allow a higher Re while ensuring a steady flow before the gust, we exploit permeability. Specifically, we consider $Da = 10^{-4}$, a range of the nondimensional mass m between 0.5 and 2, and a range of the Galilei number Ga between 10 and 50. Here, we consider $Ga \equiv Re \hat{u}_g / \hat{u}_t$ (\hat{u}_g is the gravitational velocity and \hat{u}_t is the terminal velocity) instead of Re because the gravitational velocity is known a priori, while the terminal velocity is an output of the simulation. It is noted that there is a lack of uniformity in the literature on the name of this nondimensional group, sometimes named after the first name of Galileo Galilei, i.e. Galileo number (e.g. Brandt & Coletti, 2022), and sometimes known as Archimedes number (e.g. Ern *et al.*, 2012).

The primary objectives of this study are as follows: (i) to identify the boundary between steady and unsteady kinematics of permeable plates as a function of m and Ga , (ii) to investigate the reduction of descent velocity in the transient regime when subjected to a transverse gust, and (iii) to investigate how the gust effect varies with m , Ga and the gust ratio. The remainder of the paper is structured as follows. The problem definition and the governing equations are described in §2. The numerical method and the solver setup are presented in §3. The results and discussions are presented in §4. The salient outcomes of this study are summarised in §5.

2 Problem Definition and Governing Equations

We model a 2D permeable plate with length \hat{l} and aspect ratio $\chi = 10$, falling freely under the influence of gravity (fig. 1a). The hat over the symbols is used to indicate dimensional quantities. In the following, all quantities are made nondimensional using the fluid density $\hat{\rho}$, the plate length \hat{l} , and the magnitude of the gravitational velocity \hat{u}_g , such that $\rho = l = u_g = 1$. The gravitational velocity is defined as $\hat{u}_g \equiv (\hat{m} \hat{g} / \hat{\rho} \hat{l}^2)^{1/2}$, where \hat{m} is the mass of the solid body, and \hat{g} is the gravitational acceleration. This definition is adapted from that of, for instance, Brandt & Coletti (2022) and Ern *et al.* (2012), considering that here the buoyancy is null because the body is permeable. The permeable plate model could represent, for example, a two-dimensional filamentous structure such that the volume of the impervious filaments is negligible compared to the area of the circumscribing volume, i.e. of the plate. Furthermore, as the body is permeable, we prefer considering the nondimensional body mass $m \equiv \hat{m} / \hat{\rho} \hat{l}^3$ to the density ratio.

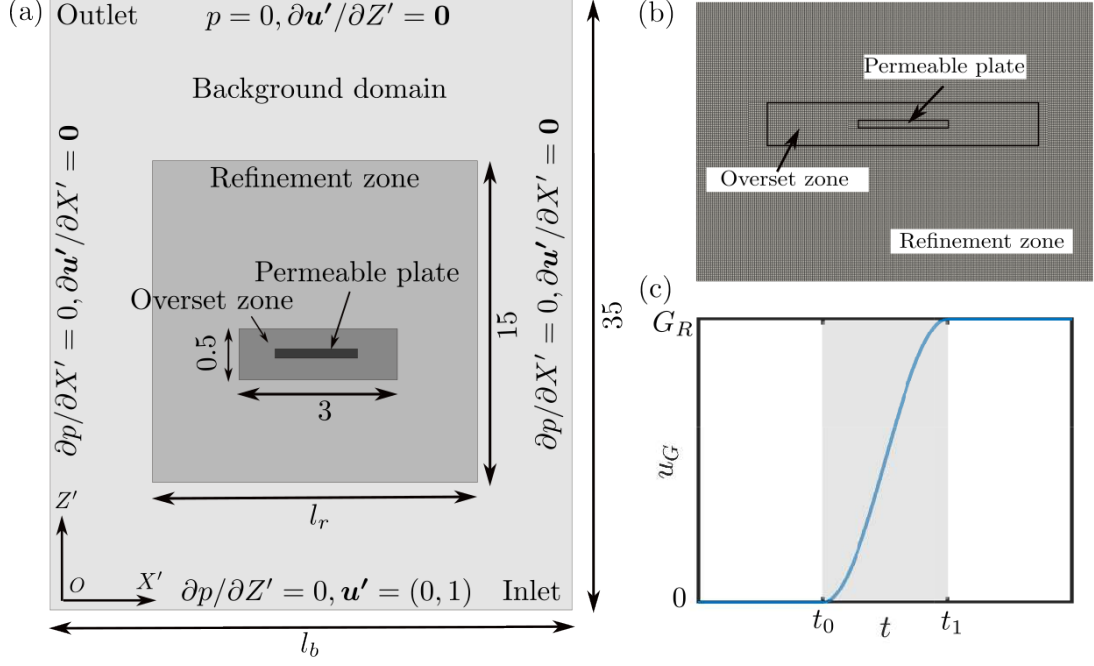


Figure 1: (a) A schematic of the computational domain (not-to-scale) and boundary conditions; (b) a zoomed section of the structured mesh around the plate; and (c) an example of transverse gust profile with $t_0 = 15$, $t_1 = 16$, and $G_R = 1$.

The flow is governed by the continuity and the Darcy equations inside of the permeable plate. In the clear fluid region around the plate, where $Da \rightarrow \infty$, the Darcy equation reduces to the incompressible Navier-Stokes equation for a Newtonian fluid. The plate motion is governed by the Newton-Euler equations. The nondimensional governing equations in an inertial frame of reference with origin at the centre of mass of the body are

$$\nabla \cdot \mathbf{u} = 0, \quad (1)$$

$$\frac{\partial \mathbf{u}}{\partial t} + (\mathbf{u} \cdot \nabla) \mathbf{u} = -\nabla p + \frac{1}{Ga} \nabla^2 \mathbf{u} - \frac{1}{GaDa} \mathbf{u}, \quad (2)$$

$$m \mathbf{u}_b + \boldsymbol{\omega}_b \times m \mathbf{u}_b = \mathbf{F} + \boldsymbol{\gamma}, \quad (3)$$

$$\mathbf{I}_0 \dot{\boldsymbol{\omega}}_b + \boldsymbol{\omega}_b \times \mathbf{I}_0 \boldsymbol{\omega}_b = \mathbf{T} + e \mathbf{r} \times \boldsymbol{\gamma}, \quad (4)$$

where \mathbf{u} is the fluid velocity; t is time, p is the kinematic pressure; \mathbf{u}_b is the body velocity; $\boldsymbol{\omega}_b$ is the body angular velocity; \mathbf{I}_0 is the body inertia tensor; \mathbf{F} and \mathbf{T} are the fluid force and torque exerted by the fluid on the body, respectively; $\boldsymbol{\gamma}$ is a unit vector in the direction of the gravity acceleration; \mathbf{r} is a unit vector from the centre of gravity to the centre of buoyancy, and e is the distance between the two centres.

3 Computational Methodology

Two-way coupled fluid-structure-interaction simulations are carried out using a finite volume approach with the overset mesh-based flow solver `overPimpleDyMFoam` in `OpenFOAM` (Jasak *et al.*, 2007). An overset mesh motion strategy is used (Guerrero, 2006; Chandar & Gopalan, 2016) with `cellVolumeWeight` interpolation. A partitioned weak coupling strategy-based six-degrees-of-freedom solver is used, where the fluid and solid solvers interact in a staggered manner. The structural solver uses a Newmark-beta time integration scheme. The spatial and temporal discretisations are second-order accurate. A preconditioned conjugate gradient iterative solver is used to solve for the pressure and cell displacement, whereas a diagonal incomplete-Cholesky method is used for preconditioning. A preconditioned smooth solver is used to solve the pressure-velocity coupling equation, and the symmetric Gauss-Seidel method is used for preconditioning.

The governing equations are solved for a noninertial frame of reference $O(X', Z')$, which translates vertically at the gravitational velocity \mathbf{u}_g , and horizontally at the gust velocity \mathbf{u}_G , with respect to (w.r.t.) an earth-fixed frame $O(X, Z)$ (fig. 1). The gust velocity is $\mathbf{u}_G = \mathbf{0}$ up to time t_0 to allow the body to settle at a constant terminal velocity, for t between t_0 and t_1 , the horizontal gust speed is

$$u_G = \frac{1}{2} \left[1 - \cos \left(\frac{\pi(t - t_0)}{t_1 - t_0} \right) \right] G_R, \quad (5)$$

where G_R is the gust ratio (fig. 1c). The gust period is $t_G \equiv t_1 - t_0$. After t_1 , the horizontal velocity is $u_G = G_R$.

Solving the equations in a noninertial frame enables the simulations to converge with a comparatively smaller domain size than in an inertial frame-of-reference due to the smaller degree of displacement of the plate. As the noninertial frame of reference does not rotate, the fictitious accelerations reduce to the uniform acceleration of the noninertial frame, $\dot{\mathbf{u}}_G = d\mathbf{u}_G/dt$. In the fluid equations (eq. 1 and 2), however, uniform body forces such as gravity are not considered and the resolved pressure p is net of the hydrostatic pressure resulting from the body forces, which does not contribute to fluid forces and torque. Instead, the fictitious acceleration is considered in Newton's equation 3 by considering $\dot{\mathbf{u}}_b = \dot{\mathbf{u}}'_b + \dot{\mathbf{u}}_G$, where $\dot{\mathbf{u}}'_b$ is the body acceleration w.r.t. the noninertial frame. This reveals that the plate perceives the gust as a horizontal force $-m\dot{\mathbf{u}}_G$ that is added to the fluid force on the right-hand side of equation 3. The correct implementation of the simulations in the noninertial frame has been verified by solving a subset of cases in an inertial frame and ensuring that identical results were achieved.

The domain size and boundary conditions in the non-inertial frame-of-reference are shown in fig. 1a. The lengths of the refinement and background regions are l_r and l_b , respectively, where $l_r = 10, l_b = 20$ for simulations with a single ramp gust and $l_r = 20, l_b = 30$ for simulations with a sustained gust. In the noninertial frame, the plate's vertical initial velocity is one, while it is zero in the earth-fixed frame. The computational domain is discretised using structured grids, of which the region near the plate is shown in fig. 1b. The whole domain is composed of the background mesh region, refinement region, overset mesh region, and permeable plate mesh region. The resolution of the refinement region mesh is the same size as that of the overset and plate mesh regions. The overset and the plate mesh regions are given the same Zone Ids. The additional Darcy sink term in eqn. 2 is incorporated within the plate cell zone at run time using the finite volume option capability of fvOptions.

The absolute error tolerance criteria for pressure and velocity are set to 10^{-7} , and the numerical uncertainty due to the spatial and temporal resolutions in the computation of the forces is assessed in less than 5%. One can refer to Bose & Viola (2023) for detailed verification and validation studies.

4 Results and Discussions

The boundary between steady and unsteady kinematics of free-falling permeable plates is identified in the parametric space of Ga and m . The parametric map of steady and unsteady plate motions is presented in fig. 2a. For this set of results, an initial disturbance is provided by means of a horizontal velocity of the plate equal to half of the gravitational velocity such that $\mathbf{u}'_b = (0.5, 1)$ at $t = 0$ in the noninertial frame-of-reference. For low values of Ga and m , the 2D permeable plates undergo a steady fall after the initial unsteady transient. As high Ga and m values, the plate kinematics tend to a periodic fluttering or tumbling. As expected, the kinematics is unsteady when the viscous forces are small compared to the gravity force and the inertia forces.

Figure 2b presents the trajectories of the plate centre of mass in the earth-fixed frame for three example cases (fig. 2a). For low Ga and m ($Ga = 10, m = 0.5$), the plate trajectory becomes a straight line after the initial transients, representing a steady fall condition. For high Ga and low m ($Ga = 50, m = 0.5$), the plate trajectory shows a damped oscillation with a decreasing envelope approaching a straight line, also indicative of a steady fall. Finally, for high Ga and high m ($Ga = 10, m = 2$), the plate trajectory shows an increasing envelope, representative of the unsteady kinematics.

It is noted that Ga is an index of the relative importance of the gravitational to the viscous force. Furthermore, for a free-falling body, where the fluid force is, on average, in equilibrium with the gravitational force, Ga also represents the relative importance of the inertia to the viscous force. Instead, m is an index of the relative importance of the gravitational force with the overall fluid forces. Consider, for example, a permeable disk with a constant mass and dimension, Ga increases with decreased fluid viscosity, while m increases with decreased

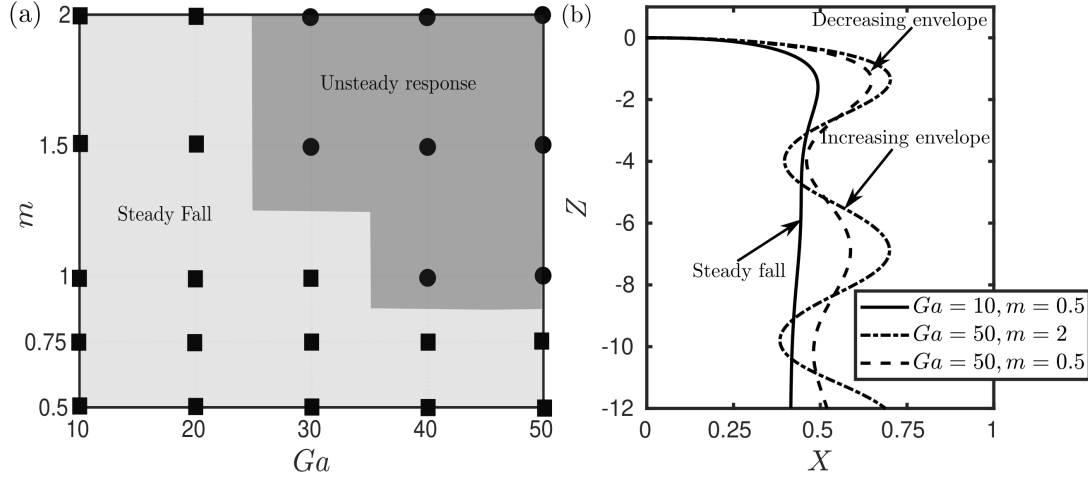


Figure 2: (a) $Ga - m$ parametric map of the flight stability; (b) plate trajectories for $Ga = 10, m = 0.5$ (stable); $Ga = 50, m = 0.5$ (stable); and $Ga = 50, m = 2$ (unstable).

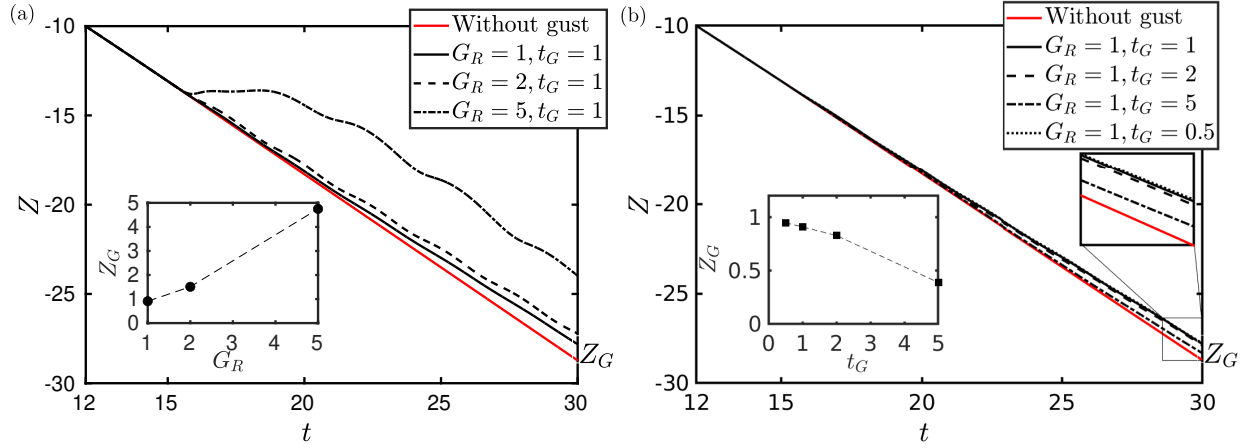


Figure 3: Effect of (a) gust ratio G_R and (b) gust period t_G on the time histories of the altitude $Z(t)$ and on the altitude gain Z_G (assessed at $t = 30$) for $Ga = 50$ and $m = 0.5$.

fluid density. The decreasing stability of the kinematics with Ga and m is consistent with the decreasing effect of the viscous fluid forces.

We now investigate the gust response in the steady fall regime. The time history of the vertical coordinate is plotted in fig. 3a for a plate with $Ga = 50$ and $m = 0.5$, experiencing a range of G_R from 1 to 5 within a constant gust period $t_G = 1$ ($t_0 = 15, t_1 = 16$). We discover that a horizontal gust results in a temporary reduction in the terminal velocity. Therefore, once the transient effect of the gust has ended, the plate is at a higher altitude than if it did not experience the gust. The difference in altitude, Z_G , which is here assessed at $t = 30$, is shown to increase monotonically with G_R (fig. 3a inset). This trend is explained by recalling that the gust is perceived as a horizontal force with magnitude $m\dot{u}_G$ (see §3), and the maximum of $m\dot{u}_G$ increases with G_R .

Thereafter, we gradually increase the gust period t_G from 0.5 to 5, for a constant gust ratio $G_R = 1$ ($t_0 = 15$ and $t_1 = 15.5, 16, 17, 20$, respectively). The time history of the vertical coordinate of the plate is plotted in fig. 3b for different t_G values. We found that Z_G decreases with increasing t_G (fig. 3b inset). In fact, as the gust period tends to infinity, the maximum gust force decreases and the dynamic response tends to quasi-steady, and thus $Z_G \rightarrow 0$. Conversely, Z_G asymptotically tends to a constant value with decreasing t_G . In fact, while the maximum gust force increases with decreasing t_G , the impulse of the force is constant.

Figure 4a shows the gust response Z_G within the $Ga - m$ parametric space for $G_R = 1$ and $t_G = 1$ (here Z_G is evaluated at $t = 35$). The maximum values of Z_G are found for high Ga and m . The highest value is 1.4 at

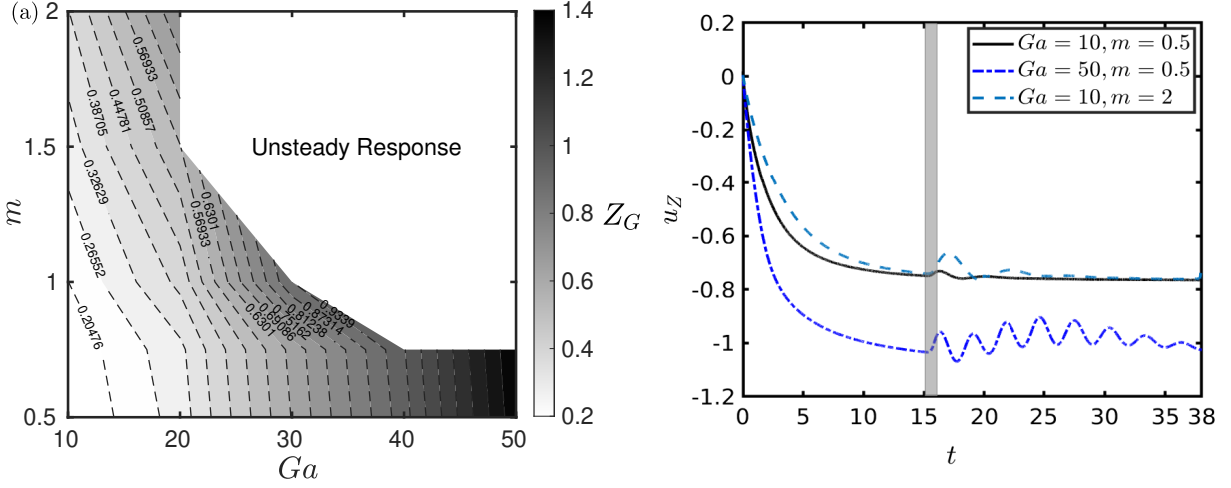


Figure 4: (a) Contour of Z_G in the $Ga - m$ parametric space at $G_R = 1$ and $t_G = 1$; (b) the gust effect on the descent velocity on three different parameter sets ($Ga = 10, m = 0.5$; $Ga = 50, m = 0.5$; and $Ga = 10, m = 2$). The grey shed area in (b) shows the gust period.

$Ga = 50, m = 0.5$. The rate of increase of Z_G is higher with increasing Ga than with increasing m .

It should be noted that permeability increases the stability of the plate and thus allows exploring the gust response at higher Ga and m values than for an impermeable plate. However, the underlying uplifting mechanism is not directly related to the permeability, and it is thus likely to occur also for impermeable bodies. Before the gust, the plate is always orthogonal to the flow.

Figure 4b presents the time histories of the plate vertical velocity u_z for three corners of the $Ga - m$ plane ($Ga = 10, m = 0.5$; $Ga = 50, m = 0.5$; and $Ga = 10, m = 2$). The grey-shaded area indicates the gust period ($t_0 = 15, t_1 = 16$). The plates are initially released with zero vertical velocity, and they reach the terminal velocity within about 10-15 convective periods t . At low Ga and m values, the gust effect is negligible and the permeable body reaches its terminal velocity after a short transient. This results in a small $Z_G \sim 0.2$. Instead, u_z undergoes a longer oscillatory transient with larger amplitude fluctuations both at high Ga and high m .

The corresponding plate trajectories for these three cases in the noninertial frame of reference are presented in figs. 5a-c, respectively. In the noninertial frame, the initial velocity of the plate is $\mathbf{u}'_b = (0, 1)$ at $t = 0$. Therefore, the plate first moves upwards and decelerates till it reaches the terminal velocity. Note that if the plate were stationary in the noninertial frame, it would imply that the terminal velocity is equal to the gravitational velocity in the earth-fixed frame.

When the gust occurs, the plate is initially displaced horizontally by the gust. Having gained some horizontal velocity, the angle of attack is now lower than $\pi/2$, but the force remains about normal to the plate and its magnitude increases because of the increased relative flow velocity experienced by the plate, resulting in a temporary upward force increase. The trajectories in figs. 5a-c reveal that the distance travelled horizontally increases with both Ga and m ; the largest pitch oscillations are observed for the highest Ga value (figs. 5b), while the maximum horizontal velocity is achieved at the highest m value (figs. 5c).

Figure 5d shows the line convolution integral of a few representative instantaneous flow fields around a free-falling permeable plate at $Ga = 50, m = 0.5$ after the transverse gust ($t_0 = 15$ and $t_1 = 16$) in the noninertial frame. The snapshot at $t = 15$ shows the instantaneous position of the plate just before the gust, where the plate is stationary in the noninertial frame and a steady separated vortex dipole exists. As the gust occurs, the plate accelerates along the negative X' direction (because it translates horizontally slower than the gust velocity). Gradually, the plate pitches and moves upwards (because it falls slower than the terminal velocity). As the gust ends, the plate continues to move in an oscillatory manner (fig. 5b). The flow field is unsteady in this transient regime, and the steady vortex dipole is formed again once the plate settles at its terminal velocity.

We now demonstrate that the horizontal gust can also uplift the plate (fig. 6a), i.e. the plate gains a positive (upwards) vertical velocity in the earth-fixed frame (fig. 6b). We consider a plate with $Ga = 10$ and $m = 2$. The gust velocity follows eq. 5 (with $G_R = 5, t_0 = 15$ and $t_1 = 16$) up to half of the gust period ($t = 15.5$), and

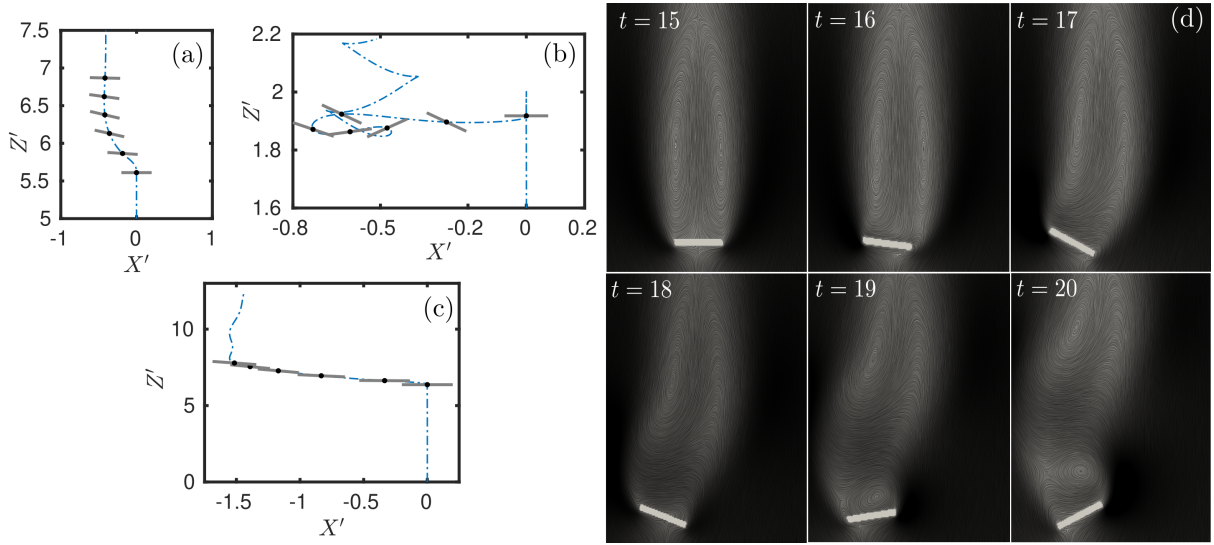


Figure 5: Trajectories of the plate for (a) $Ga = 10, m = 0.5$; (b) $Ga = 50, m = 0.5$; (c) $Ga = 10, m = 2$; and (d) representative snapshots of the instantaneous line convolution integral visualisation of the wake of the plate at $Ga = 50, m = 0.5$ in the noninertial frame-of-reference when subjected to a gust with $G_R = 1$ and $t_G = 1$. Plate positions are shown at $t = 15$ to 20 with an interval of $t = 1$ in subfigs. a-d.

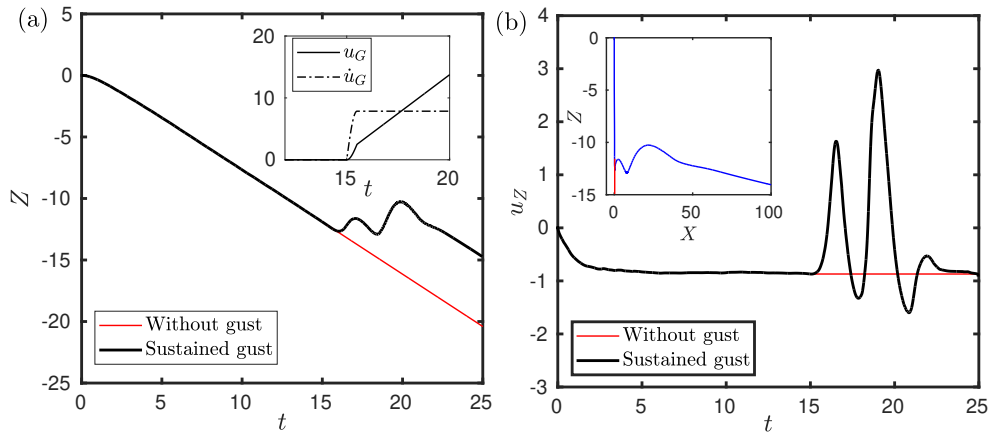


Figure 6: (a) The time history of the vertical earth-fixed coordinate of the plate, and (b) the vertical velocity. The gust velocity and acceleration are shown in the inset of subfig. a, and the trajectory of the plate are shown in the inset of subfig. b.

then it continues to increase linearly, resulting in a constant gust acceleration of $\dot{u}_G = 7.85$ (fig. 6 inset). The time history of the plate altitude (Z) and of the vertical velocity (u_Z) are plotted in fig. 6a-b, respectively, while the inset of fig. 6b shows the trajectory in the earth-fixed frame. These results reveal that a free-falling plate can gain substantial height in response of a *horizontal* gust, gaining an upward vertical velocity that is multiple times its terminal velocity in quiescent flow.

5 Concluding Remarks

The flight dynamics and gust response of 2D permeable plates are investigated for a range of the Galilei number Ga (10 to 50) and the nondimensional mass ratio m (0.5 to 2), and a constant value of the Darcy number $Da = 10^{-4}$. The fluid-structure interaction simulations are carried out by weakly coupling a finite volume solver, where the flow through the plate is modelled with the Darcy equation and a six-degree-of-freedom structural solver. The equations are solved in a noninertial frame of reference, moving vertically with the gravitational velocity and horizontally with the gust velocity.

The $Ga - m$ parametric space is first investigated to identify the boundary between steady and unsteady of the kinematics of free-falling plates in quiescent flow without gusts. We show that 2D permeable plates exhibit a steady fall in the low values of Ga and m , while the kinematics is unsteady for high Ga and/or high m .

We then investigate the effect of transverse (horizontal) gusts on the plate motion with Ga and m values within the steady fall region. Gusts are modelled as a cosine ramp increase of the horizontal flow velocity. We show that the horizontal gust results in a transient reduction of the terminal velocity. The gust effect is quantitatively measured through the difference in altitude after the transient between a plate that experiences a gust and one that falls in quiescent flow. The gain in altitude increases with the gust acceleration, as well as with Ga and m .

Finally and importantly, we show that a sufficiently large and sustained gust can result in a temporary uplift of the plate. These results might contribute to understanding the effect of turbulence on the dispersal of inertial particles and will inform the design of insect-scale flyers transported and distributed by the wind.

Funding. This work was supported by the European Research Council through the Consolidator Grant 2020 “Dandidrone: a Dandelion-Inspired Drone for Swarm Sensing” [H2020 ERC-2020-COG 101001499].

Acknowledgements. This work used the Cirrus UK National Tier-2 HPC Service at EPCC funded by the University of Edinburgh and EPSRC (EP/P020267/1).

Deceleration of Interests. The authors report no conflict of interest.

References

- BI, DIANFANG, LU, JIAXING, WEI, YINGJIE, SUN, TIEZHI & OTHERS 2022 Numerical analysis of factors influencing freely falling annular disks in an infinite fluid. *Physical Review Fluids* **7** (5), 054702.
- BOSE, C & VIOLA, I, M 2023 Porous plates at incidence. *ArXiv*, /abs/2303.13296 .
- BRANDT, LUCA & COLETTI, FILIPPO 2022 Particle-laden turbulence: Progress and perspectives. *Annual Review of Fluid Mechanics* **54**, 159–189.
- CASTRO, IP 1971 Wake characteristics of two-dimensional perforated plates normal to an air-stream. *Journal of Fluid Mechanics* **46** (3), 599–609.
- CHANDAR, DOMINIC D & GOPALAN, HARISH 2016 Comparative analysis of the arbitrary mesh interface (ami) and overset methods for dynamic body motions in openfoam. In *46th AIAA Fluid Dynamics Conference*, p. 3324.
- CUMMINS, CATHAL, SEALE, MADELEINE, MACENTE, ALICE, CERTINI, DANIELE, MASTROPAOLO, ENRICO, VIOLA, IGNAZIO MARIA & NAKAYAMA, NAOMI 2018 A separated vortex ring underlies the flight of the dandelion. *Nature* **562** (7727), 414–418.
- CUMMINS, CATHAL, VIOLA, IGNAZIO MARIA, MASTROPAOLO, ENRICO & NAKAYAMA, NAOMI 2017 The effect of permeability on the flow past permeable disks at low reynolds numbers. *Physics of Fluids* **29** (9), 097103.
- ERN, PATRICIA, RISSO, FRÉDÉRIC, FABRE, DAVID & MAGNAUDET, JACQUES 2012 Wake-induced oscillatory paths of bodies freely rising or falling in fluids. *Annual Review of Fluid Mechanics* **44**, 97–121.

- FIELD, STUART B, KLAUS, M, MOORE, MG & NORI, FRANCO 1997 Chaotic dynamics of falling disks. *Nature* **388** (6639), 252–254.
- GALLER, JOSHUA N & RIVAL, DAVID E 2021 Characterization of milkweed-seed gust response. *Bioinspiration & Biomimetics* **16** (6), 066017.
- GUERRERO, JOEL 2006 Overset composite grids for the simulation of complex moving geometries. *DICAT, University of Genoa, Italy*.
- IYER, VIKRAM, GAENSBAUER, HANS, DANIEL, THOMAS L & GOLLAKOTA, SHYAMNATH 2022 Wind dispersal of battery-free wireless devices. *Nature* **603** (7901), 427–433.
- JASAK, HRVOJE, JEMCOV, ALEKSANDAR & TUKOVIC, ZELJKO 2007 OpenFOAM: A C++ library for complex physics simulations. In *International workshop on coupled methods in numerical dynamics*, pp. 1–20.
- KAJIKAWA, MASAHIRO 1982 Observation of the falling motion of early snow flakes part i. relationship between the free-fall pattern and the number and shape of component snow crystals. *Journal of the Meteorological Society of Japan. Ser. II* **60** (2), 797–803.
- KIM, BONG HOON, LI, KAN, KIM, JIN-TAE, PARK, YOONSEOK, JANG, HOKYUNG, WANG, XUEJU, XIE, ZHAOQIAN, WON, SANG MIN, YOON, HONG-JOON, LEE, GEUMBEE & OTHERS 2021 Three-dimensional electronic microfliers inspired by wind-dispersed seeds. *Nature* **597** (7877), 503–510.
- LEDDA, P. G., SICONOLFI, L., VIOLA, F., CAMARRI, S. & GALLAIRE, F. 2019 Flow dynamics of a dandelion pappus: A linear stability approach. *Physical Review Fluids* **4**, 1–8.
- LEDDA, PIER GIUSEPPE, SICONOLFI, LORENZO, VIOLA, FRANCESCO, GALLAIRE, FRANÇOIS & CAMARRI, SIMONE 2018 Suppression of von kármán vortex streets past porous rectangular cylinders. *Physical Review Fluids* **3** (10), 103901.
- LEE, MINHYEONG, LEE, SEUNG HUN & KIM, DAEGYOUN 2020 Stabilized motion of a freely falling bristled disk. *Physics of Fluids* **32** (11), 113604.
- LEE, SEUNG HUN & KIM, DAEGYOUN 2021 Aerodynamic response of a bristled wing in gusty flow. *Journal of Fluid Mechanics* **913**, A4.
- MARCHILDON, EK, CLAMEN, A & GAUVIN, WH 1964 Drag and oscillatory motion of freely falling cylindrical particles. *The Canadian Journal of Chemical Engineering* **42** (4), 178–182.
- REZAEI, T & SADEGHY, K 2019 Effect of porosity on the settling behavior of a 2d elliptic particle in a narrow vessel: A lattice-boltzmann simulation. *Physics of Fluids* **31** (12), 123301.
- SAHA, ARUN K 2007 Far-wake characteristics of two-dimensional flow past a normal flat plate. *Physics of Fluids* **19** (12), 128110.
- SMITH, EH 1971 Autorotating wings: an experimental investigation. *Journal of Fluid Mechanics* **50** (3), 513–534.
- VAGNOLI, GIOVANNI, ZAMPOGNA, G.A., CAMARRI, S., GALLAIRE, F. & LEDDA, P.G. 2023 Permeability sets the linear path instability of buoyancy-driven disks. *Journal of Fluid Mechanics* **955**, A29.
- VIETS, HERMANN & LEE, DA 1971 Motion of freely falling spheres at moderate reynolds numbers. *AIAA Journal* **9** (10), 2038–2042.
- VINCENT, LIONEL, SHAMBAUGH, W SCOTT & KANSO, EVA 2016 Holes stabilize freely falling coins. *Journal of Fluid Mechanics* **801**, 250–259.
- VIOLA, IGNAZIO MARIA & NAKAYAMA, NAOMI 2022 Flying seeds. *Current Biology* **32**, R204–R205.
- WIESEMÜLLER, FABIAN, MENG, ZIWEN, HU, YIJIE, FARINHA, ANDRE, GOVDELI, YUNUS, NGUYEN, PHAM H, NYSTRÖM, GUSTAV & KOVAC, MIRKO 2022 Transient bio-inspired gliders with embodied humidity responsive actuators for environmental sensing. *Frontiers in Robotics and AI* **9**.
- WILLMARTH, WILLIAM W, HAWK, NORMAN E & HARVEY, ROBERT L 1964 Steady and unsteady motions and wakes of freely falling disks. *The physics of Fluids* **7** (2), 197–208.
- YOON, HONG-JOON, LEE, GEUMBEE, KIM, JIN-TAE, YOO, JAE-YOUNG, LUAN, HAIWEN, CHENG, SHYUAN, KANG, SOOHYEON, HUYNH, HUONG LE THIEN, KIM, HYEONSU, PARK, JAEHONG & OTHERS 2022 Biodegradable, three-dimensional colorimetric fliers for environmental monitoring. *Science Advances* **8** (51), eade3201.
- ZHANG, WENHUI, BI, DIANFANG & WEI, YINGJIE 2023 Falling styles of perforated disks. *International Journal of Multiphase Flow* **161**, 104401.